Polymorphic magnetization and local ferromagnetic structure in Co-doped Mn$_2$NiGa alloys

L. Ma (马丽),[1,2] W. H. Wang (王文洪),[1] C. M. Zhen (甄聪棉),[2] D. L. Hou (侯登录),[2] X. D. Tang (唐晓丹),[1]
E. K. Liu (刘恩克),[1] and G. H. Wu (吴光恒)[1,*]

[1]*Beijing National Laboratory for Condensed Matter Physics, Institute of Physics, Chinese Academy of Sciences, Beijing 100190, China*
[2]*Department of Physics, Hebei Advanced Thin Films Laboratory, Hebei Normal University, Shijiazhuang 050016, China*
(Received 4 May 2011; published 9 December 2011)

Polymorphic magnetization behavior has been observed experimentally in the Heusler alloy Mn$_2$NiGa in which Co has been substituted for Ni or Ga. The magnetization of the austenitic phase can be enhanced up to 132 emu/g, when more than 50% of the antiferromagnetic couplings between Mn atoms are changed to ferromagnetic couplings at the largest composition tolerance for Co substituting for Ga. The effects of the exchange interaction have been investigated based on the corresponding atomic configuration generated by the occupation selectivity of the doped Co atoms. First-principles calculations indicate that a high level of d-electron hybridization can occur when Mn atoms are the nearest neighbors of a Co atom. This causes a strong ferromagnetic exchange interaction in specific atomic configurations and produces a local ferromagnetic structure in the native ferrimagnetic structure matrix. It has been indicated that, based on theoretical work of Stearns, the interatomic distance plays a critical role in producing the local ferromagnetic structure. This has also been used to explain the magnetization behavior through the martensitic transformation in Mn$_2$NiCoGa alloys.

PACS number(s): 75.20.En

I. INTRODUCTION

Heusler-type ferromagnetic shape-memory alloys (FSMAs) have become very attractive candidates for high-performance magnetic actuator materials since the time that magnetic-field-induced martensitic transformations were observed in several alloys, such as NiCoMnIn,[1] NiCoMnSn,[2,3] NiCoMnSb,[4] NiCoMnGa,[5] MnCoNiGa,[6] and NiMnCoAl.[7] Without Co content, these alloys usually exhibit a low magnetization because their Mn-rich composition generally gives rise to a ferrimagnetic structure. From the thermodynamics point of view, obtaining a large magnetization difference (ΔM) between the parent phase and the martensitic phase is crucial. In the studies cited above, in order to obtain sufficient Zeeman energy ΔMH to induce the martensitic transformation, Co was doped into the alloys to maximize the value of ΔM. The efficacy of Co is due to the facts that (i) the Co-Mn exchange interaction can turn the antiferromagnetic coupling between Mn atoms into a ferromagnetic coupling and achieve a high magnetization in the parent phase[8] and that (ii) such an exchange interaction can be inoperative in the martensite phase and result in a low magnetization. A large ΔM between the parent phase and the martensitic phase can therefore be achieved. However, the physical mechanism for such different exchange interactions in the two phases has not been investigated systemically.

In this paper, the exchange interaction between the magnetic Co, Mn, and Ni atoms has been investigated by changing the atomic configuration in the alloy. Mn$_2$NiGa, containing the largest Mn content and having an Hg$_2$CuTi structure in Heusler alloys,[9] has been utilized as a mother composition. From this composition, two different atomic configurations can be realized experimentally by substituting Co for Ni or Ga, respectively. In these two different configuration models, the interatomic distance between the Co and Mn atoms, which are the main carriers of the magnetic moment, is different. Based on this fact, we have shown that the magnetic exchange interaction in this system is mainly determined by

two factors: the kind of the magnetic atoms and the interatomic distance. This viewpoint enables us to explain what exchange interactions create the high magnetization in the parent phase following doping with Co. Furthermore, this understanding is also applicable to explaining why this interaction effect becomes inoperative in the martensitic phase. In fact, polymorphic magnetization behavior has been observed in this work in which the magnetization can be manipulated by a factor of three by varying the atomic configuration.

Based on the different atomic occupations in the MnCoNiGa alloys, a series of *ab initio* calculations has been carried out in the present work, and the results confirm that (1) d-electron hybridization can be enhanced when the Mn atom is surrounded by Co atoms; (2) two main magnetic couplings, Mn-Mn and Mn-Co, co-dominate the magnetic structure and magnetization in Mn$_2$Co$_x$Ni$_{1-x}$Ga and Mn$_2$Co$_x$NiGa$_{1-x}$ alloys; (3) a local ferromagnetic structure is formed in the ferrimagnetic matrix surrounding the Co atoms, which dramatically increases the magnetization in Mn$_2$Co$_x$NiGa$_{1-x}$ alloys due to its special atomic configuration. Furthermore, we have confirmed the relative strengths of the exchange interactions between Mn-Mn, Mn-Co, and Mn-Ni based on the work of Stearns and explained the formation conditions of the local ferromagnetic structure in Mn$_2$Co$_x$NiGa$_{1-x}$ alloys. In order to explain the appearance of the low magnetization ferrimagnetic structure in the martensitic phase, we show that the interatomic distance becomes a key factor which determines the fate of the local ferromagnetic structure after a lattice variation.

The paper is organized as follows: Sec. II contains details concerning the methods of the experiment and the calculation. Section III presents the experimental and calculated results and related discussion, including: (1) the magnetization; (2) the crystal structure and atomic configurations; (3) electronic structure and spin moments; (4) the exchange interaction and magnetic structure; and (5) the behavior of the local ferromagnetic structure across the crystallographic and magnetic transition. Finally, the paper is summarized in Sec. IV.

II. EXPERIMENTAL AND COMPUTATIONAL DETAILS

Based on the mother composition Mn_2NiGa, two series of samples of $Mn_2Co_xNiGa_{1-x}(x = 0 \sim 0.52)$ and $Mn_2Co_xNi_{1-x}Ga$ ($x = 0 \sim 0.50$) in which, respectively, the Co chemically substitutes for Ni or Ga, were prepared by arc melting of Mn, Ni, Co, and Ga metals with purity of 99.95% in an argon atmosphere. These MnCoNiGa ingots were heat-treated at $920\,°C$ for 24 h in order to homogenize the distribution of the constituents throughout the alloys. Because a second face-centered cubic (*fcc*) structure emerged in the ingots of $Mn_2Co_xNiGa_{1-x}$ with $x \geqslant 0.24$, the melt-spinning technique was adopted for alloys with $x \geqslant 0.24$.[10] In order to ensure high chemical ordering, the homogenized and spun samples were further annealed at $650\,°C$ for 72 h and subsequently quenched in an ice-water mixture. The structures of the samples were determined by using x-ray diffraction (XRD) with Cu $K\alpha$ radiation ($\lambda = 1.5418$ Å) from the ground powder at room temperature. Here, ac magnetic susceptibility measurements were performed to determine the Curie temperature, T_C. The low temperature (5 K) saturation magnetization values, M_S were measured in fields up to 50 kOe using a SQUID magnetometer (SQUID-Quantum Design).

The electronic structures of the two series of alloys were calculated using the self-consistent full-potential linearized-augmented plane-wave (FP-LAPW) method based on the generalized gradient approximation within the density functional theory,[11,12] where the potential and/or the charge density in the crystal are treated with no shape approximations. Sixty k points in the irreducible Brillouin zone were used to achieve self consistency in the calculation. The self consistency was found to be better than 0.01 meV/a.u. for the charge and spin densities, and the stability was better than 0.1 mRy for the total energy per cell. Supercells with $2 \times 2 \times 2$ based on the primitive unit cell were built for the calculations. The muffin-tin sphere radii R were chosen as 2.2 a.u. for the Mn and Co and 2.4 a.u. for the Ni and Ga atoms, respectively. The density plane-wave cutoff was taken to be $Rk_{max} = 8.0$. The electron states were treated in a scalar relativistic approximation. Using the energy eigenvalues and eigenvectors at these points, the density of states was determined by the tetrahedral integration method.[13]

III. RESULTS AND DISCUSSIONS

A. Magnetization

The lattice parameters and magnetic properties for the two series of MnCoNiGa samples studied are shown in Table I and the figures that follow. Since the enlarged ΔM comes only from the enhancement of magnetization in the parent phase by doping with Co,[6] studying the effects of doping on the magnetic structure requires that the studied object keep a stable *bcc* structure over the whole doping range. Due to the addition of Co, however, only the samples with mother composition and the smallest Co content ($x = 0.08$) retain the property of undergoing a martensitic transformation. The other samples with $x \geqslant 0.16$ do not exhibit the martensitic transformation property.

Figure 1 shows the dependence on the Co content of the molecular moments calculated from the values of M_S for the two series of MnCoNiGa samples. When the Co atoms substitute for Ni in $Mn_2Co_xNi_{1-x}Ga$ alloys, the moment increases linearly and slowly with increasing Co content. On the other hand, when the Co atoms substitute for Ga in $Mn_2Co_xNiGa_{1-x}$ alloys, the moment increases very rapidly.

TABLE I. The saturated magnetization (M_S) measured at 5 K, molecular magnetic moment (m) calculated from M_S, the Curie temperature (T_C), and lattice constant at room temperature (a), experimentally measured for the MnCoNiGa samples with compositions shown in column one.

Compounds	M_S (emu/g)	m (μ_B/f.u.)	T_C (K)	a (Å)
Mn_2NiGa	27.7[a]	1.18[a]	538	5.8782
$Mn_2Co_{0.08}Ni_{0.92}Ga$	28.4[a]	1.21[a]	546	5.8796
$Mn_2Co_{0.16}Ni_{0.84}Ga$	34.0	1.45	555	5.8808
$Mn_2Co_{0.20}Ni_{0.8}Ga$	34.6	1.48	560	5.8817
$Mn_2Co_{0.24}Ni_{0.76}Ga$	35.3	1.51	564	5.8823
$Mn_2Co_{0.32}Ni_{0.68}Ga$	36.8	1.57	571	5.8834
$Mn_2Co_{0.40}Ni_{0.60}Ga$	38.2	1.64	580	5.8836
$Mn_2Co_{0.44}Ni_{0.56}Ga$	38.9	1.65	584	5.8838
$Mn_2Co_{0.50}Ni_{0.50}Ga$	40.0	1.70	590	5.8843
$Mn_2Co_{0.08}NiGa_{0.92}$	28.1[a]	1.22[a]	533	5.8450
$Mn_2Co_{0.16}NiGa_{0.84}$	59.1	2.50	526	5.8683
$Mn_2Co_{0.20}NiGa_{0.80}$	65.5	2.77	520	5.8915
$Mn_2Co_{0.24}NiGa_{0.76}$	72.1	3.04	516	5.8637
$Mn_2Co_{0.28}NiGa_{0.72}$	79.1	3.33	517	5.8781
$Mn_2Co_{0.32}NiGa_{0.68}$	86.4	3.63	518	5.8587
$Mn_2Co_{0.40}NiGa_{0.60}$	104.3	4.37	526	5.8524
$Mn_2Co_{0.42}NiGa_{0.58}$	108.9	4.56	528	5.86778
$Mn_2Co_{0.44}NiGa_{0.56}$	115.5	4.83	530	5.8472
$Mn_2Co_{0.50}NiGa_{0.50}$	126.9	5.29	535	5.8431
$Mn_2Co_{0.52}NiGa_{0.48}$	132.1	5.50	537	5.8691

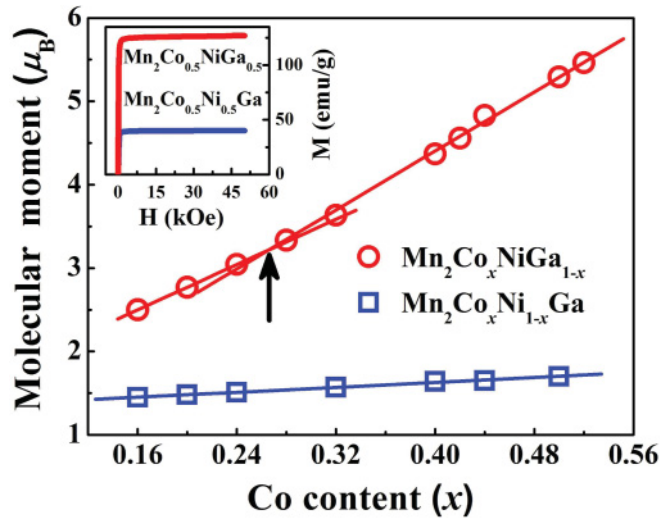[a]Martensite transformed at 270 K for Mn_2NiGa, 125 K for $Mn_2Co_{0.08}Ni_{0.92}Ga$, and 103 K for $Mn_2Co_{0.08}NiGa_{0.92}$.

FIG. 1. (Color online) The dependence on the Co content of the molecular moments for the two series of samples of $Mn_2Co_xNiGa_{1-x}$ ($x = 0.16$–0.52) and $Mn_2Co_xNi_{1-x}Ga$ ($x = 0.16$–0.50). The straight lines indicate the least-squares fitting results. The inset shows typical magnetization curves.

The latter curve can be approximately fitted with two linear dependences intersecting at about $x = 0.25$. As shown in the inset, the saturated magnetization for the two typical alloys $Mn_2Co_{0.5}Ni_{0.5}Ga$ and $Mn_2Co_{0.5}NiGa_{0.5}$ are 40 and 126.9 emu/g, respectively. They have the same content of doped Co but magnetizations that differ by a factor three. Thus, the same Co content with the different substitution styles leads to a polymorphic magnetization behavior. The largest molecular moment, 5.5 μ_B (132 emu/g), was obtained by substituting Co for Ga at the largest composition tolerance of $x = 0.52$ in the $Mn_2Co_{0.52}NiGa_{0.48}$ sample. Above this content, the second phase would appear and the pure cubic phase could not be obtained.

By fitting the two curves in Fig. 1 to calculate the moment increment, $\Delta m = \Delta M/x$ (where the ΔM denotes the increment of molecular moment), it was found that Δm_{Ni} was 0.74 μ_B in $Mn_2Co_xNi_{1-x}Ga$ alloys, while there were two large values for Δm_{Ga}, 6.79 μ_B for $x \leq 0.24$ and 8.85 μ_B for the higher Co content in $Mn_2Co_xNiGa_{1-x}$ alloys. The latter value is more than 10 times larger than Δm_{Ni}.

Corresponding to the austenitic phase, Mn_2NiGa has a ferrimagnetic structure. This alloy undergoes a martensitic transition near room temperature. The ferrimagnetic structure is based on one set of Mn atoms with a moment of -2.20 μ_B coupling in an antiparallel fashion with the other set of Mn atoms together with the Ni with moments with 3.15 and 0.27 μ_B, respectively.[10,14,15] In Mn_2CoGa systems, the Co atom has a moment of about 0.92 μ_B, larger than that of Ni.[10] Taking into account the slight influence of Co on the Mn moment, it is reasonable to believe that the Δm_{Ni} should just be the net increase of the molecular moment due to the substitution of Co for the displaced Ni. This means that the system should still retain the ferrimagnetic structure with Co substituting for Ni. Turning to the other substitution style (Co chemically substituting for Ga), such a large Δm_{Ga} cannot be understood in this simple manner. In particular, obtaining

such a large Δm_{Ga} appears to require a change from the native ferrimagnetic structure to an altered ferromagnetic one, as discussed in the following.

B. Structure and atomic configuration

In this paper, the structure of the MnCoNiGa samples has been determined by XRD methods. As shown in Fig. 2(a), the XRD of the stoichiometric Mn_2NiGa sample shows a typical Hg_2CuTi structure with the main (220), (400), and (422) reflection peaks and the (111), (200), and (311) super-lattice peaks. For the case where Co partly substitutes for Ni, the XRD patterns (not shown) are similar to that for Mn_2NiGa, which indicates that this series of samples can be easily synthesized as an off-stoichiometrical Hg_2CuTi phase by the arc-melting method. In contrast, for the case where Co partly substitutes for Ga, the *fcc* phase was found when the Co concentration exceeded $x = 0.24$, as shown in Fig. 2(b). Utilizing the melt-spinning method to prepare ribbon samples, the *fcc* phase can be eliminated completely in this series of samples until x is around 0.50,[10] as shown in Fig. 2(c).

Figure 3 shows the dependence of the lattice parameters on the Co content in the two cases of Co substituting for Ni or Ga. Stoichiometric Mn_2NiGa has lattice parameters $a = b = c = 5.8782$ Å as measured in this paper. Substituting Co for Ni, the *bcc* lattice parameters show a small and linear increase of about 0.1% over the range $x = 0$–0.5. This is due to the atomic radius of Co (1.67 Å) being slightly larger than that of Ni (1.62 Å). In the case of Co chemically substituting for Ga, the lattice parameter has a relatively large decrease of about 0.6% over the same composition range because the radius of the Co atom is much smaller than that of the Ga atom (1.81 Å). A similar phenomenon has also been observed in other Heusler alloys.[16] The best linear fit to these experimental data has been used to produce the ideal lattice parameters for the electronic structure calculations discussed below.

In order to facilitate discussion of the atomic configurations in the two series of samples, the crystallographic structures of stoichiometric Mn_2NiGa and Co-doped alloys are illustrated
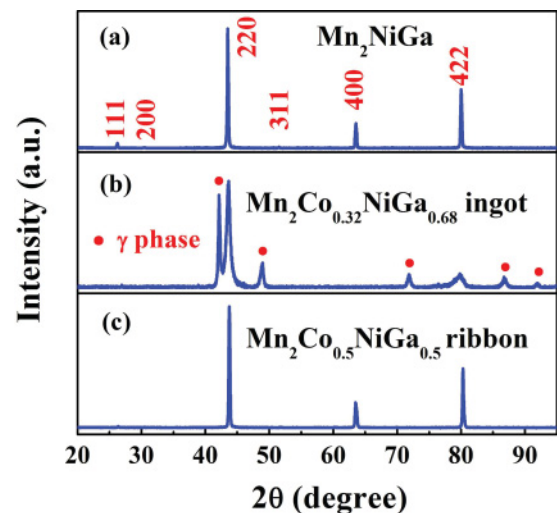

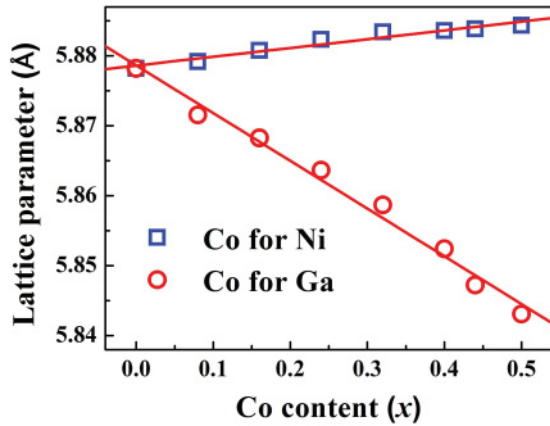FIG. 2. (Color online) X-ray diffraction patterns for (a) Mn_2NiGa and (b) $Mn_2Co_{0.32}NiGa_{0.68}$ arc-melted ingot samples, and for (c) $Mn_2Co_{0.5}NiGa_{0.5}$ melt-spun ribbon.

FIG. 3. (Color online) The Co composition dependence of the lattice parameters in $Mn_2Co_xNi_{1-x}Ga$ and $Mn_2Co_xNiGa_{1-x}$ alloys measured at room temperature.

as four configuration models in Fig. 4. The Hg_2CuTi structure has a T_d symmetry (space group 216: $F\text{-}43m$),[9,15] as shown in Fig. 4(a) (Model1). In this case, the Mn atoms occupy the nonequivalent $4a$ and $4c$ Wyckoff positions at (0, 0, 0) (denoted as MnI) and (1/4, 1/4, 1/4) (denoted as MnII), respectively. The Ni and Ga atoms are located at the $4b$ (1/2, 1/2, 1/2) and $4d$ (3/4, 3/4, 3/4) positions, respectively.
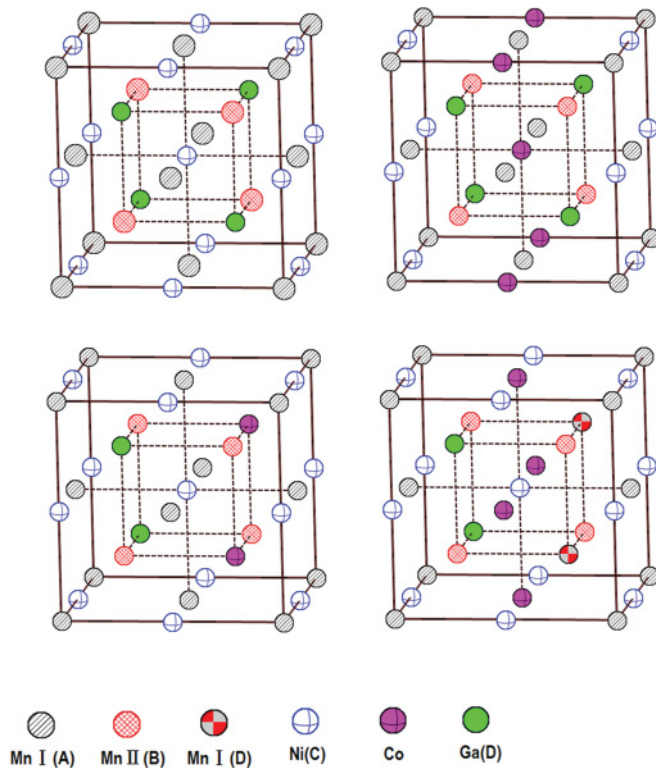

FIG. 4. (Color online) (a) The atomic configuration of stoichiometric Mn_2NiGa, (b) Co occupying the Ni site in $Mn_2Co_{0.5}Ni_{0.5}Ga$ alloy, and (c) Co occupying the Ga site in $Mn_2Co_{0.5}NiGa_{0.5}$ alloy. Part (d) shows another possible configuration for the $Mn_2Co_{0.5}NiGa_{0.5}$ alloy in which Co occupies the MnI(A) site and the corresponding MnI atom is displaced to the vacant Ga(D) site. The configurations shown in parts (a)–(d) are denoted in the text as Model1–Model4, respectively.
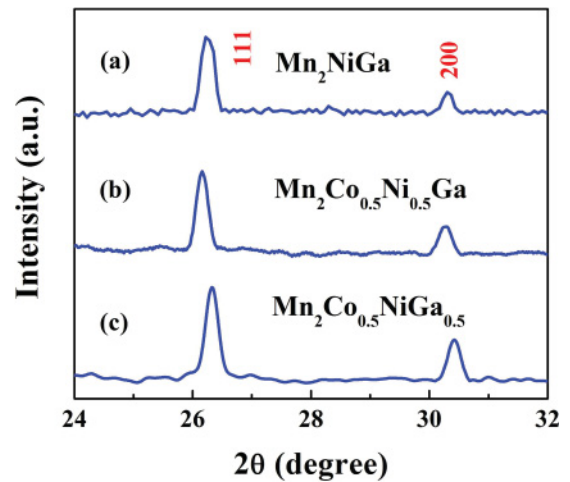

FIG. 5. (Color online) X-ray diffraction patterns for superlattice peaks of stoichiometric (a) Mn_2NiGa, (b) $Mn_2Co_{0.5}Ni_{0.5}Ga$, and (c) $Mn_2Co_{0.5}NiGa_{0.5}$.

If the atomic occupation of Co is consistent with chemical substitution, that is to say, Co occupies the substituted atomic site, the two series of samples will take up configurations in which Co occupies an Ni site in the $Mn_2Co_{0.5}Ni_{0.5}Ga$ alloy, as shown in Fig. 4(b) (Model2) and Co occupies a Ga site in the $Mn_2Co_{0.5}NiGa_{0.5}$ alloy, as shown in Fig. 4(c) (Model3). Considering the possibility of the Co occupation not being consistent with chemical substitution,[17,18] we have also assumed another configuration for the $Mn_2Co_{0.5}NiGa_{0.5}$ alloy: Co occupies the MnI(A) site and the corresponding MnI atom is displaced to occupy the vacant Ga(D) site (denoted as the MnD atom), as shown in Fig. 4(d) (Model4).

The atomic ordering configuration in the MnCoNiGa system has been experimentally observed in the present work. As shown in Fig. 5, the Mn_2NiGa sample exhibits a typical Hg_2CuTi-type chemical order in the superlattice patterns with a strong (111) peak and a relatively small (200) peak [Fig. 5(a)].[15] Due to the structure amplitude $F(200) = 4|f_A - f_B + f_C - f_D|$ and to the fact that the A and B sites are both occupied by Mn atoms, the low intensity of the (200) peak comes only from the reflection of atomic sites C and D.[19] When Co chemically substitutes for Ni in $Mn_2Co_xNi_{1-x}Ga$ alloys, the resulting superlattice peaks are very similar to those of Mn_2NiGa [Fig. 5(b)], because the reflection factors of Co and Ni atoms are very similar. The relatively small size of the (200) peak therefore means that the Co atoms occupied the Ni sites. In this case, chemical substitution leads to a consistent atomic occupation behavior. This corresponds to Model2.

However, turning to the case where the Co chemically substitutes for Ga in $Mn_2Co_xNiGa_{1-x}$ alloys, the (200) peak is larger relative to the (111) peak than in the case where Co replaced Ni. See Fig. 5(c). This implies that there should be some additional contribution coming from reflection from the A and B sites.[19] That is to say, here the A and B sites are not entirely occupied by Mn atoms, but rather there are some other atoms occupying the A and B sites. Therefore, this observation strongly suggests that, in the case of Co substituting for Ga, chemical substitution is not consistent with the actual atomic occupation and that a more complex substitution occurs.

A rule for the selectivity of atomic occupation in Heusler alloys is as follows: the doped transition metal atoms will tend preferentially to occupy the A and C sites if they have a relatively larger number of valence electrons, while those with a relatively smaller number of valence electrons will preferentially occupy the B and D sites.[17,18,20–22] In Mn_2YZ ($Y =$ Ti, V, Cr, Mn, Fe, and Co; $Z =$ Al, Ga, In, Si, Ge, Sn, and Sb) Heusler alloys, this atomic occupation rule is well followed.[10,22–26] Free energy calculations for the electronic structure of Heusler alloys also confirmed the validity of this rule.[17,27]

In the present work, the valence electron number of Co is greater than that of Mn but smaller than that of Ni. This character results in a selectivity for Co atoms to occupy a particular atomic site when they are chemically doped in the Mn_2NiGa system: the Co atoms will occupy the Ni sites when Co substitutes for Ni and will go to the Mn sites when Co substitutes for Ga. Our calculation about the total energy of the system also indicates the validity of this selectivity. Thus, based on our XRD experimental observation and the above discussion, we can confirm that the atomic configuration in $Mn_2Co_xNiGa_{1-x}$ alloys should be that of Model4 instead of Model3, as illustrated in Figs. 4(d) and 4(c), respectively. This selectivity is also confirmed by our electronic structure calculations, as shown in the next section.

C. Calculated electronic structure and spin moment

First-principles calculations have been carried out to study the magnetic properties in the two series of alloys. Four atomic configurations have been calculated: (1) stoichiometric Mn_2NiGa with the Hg_2CuTi structure (Model1); (2) Co chemically substituting for Ni (Model2); (3) Co chemically substituting for Ga with the atomic configuration of Model4; and (4) Model3, for comparison with Model4, assuming that the Co atoms follow the chemical substitution trend and directly occupy the vacant Ga (D) sites. These calculated results provide us with more detailed information about the electronic structure, the magnetic structure, and the magnetic moments for the total molecule and for each kind of atom separately.

Figures 6–8 show the densities of states (DOS) for the spin-up (majority) and the spin-down (minority) electrons for three typical compositions. One strong peak for a Ga atom at about -15.50 eV is not shown since it is symmetric between spin-up and spin-down states and therefore does not contribute to the total moment. As shown in Fig. 6(a), the DOS for the stoichiometric Mn_2NiGa mother alloy indicates a ferrimagnetic ground state which is mainly structured by the moment of MnI in antiparallel alignment with that of MnII.[14,15]

In Model2 where Co substitutes for Ni and occupies the vacant Ni(C) site, the DOS for $Mn_2Co_{0.25}Ni_{0.75}Ga$ and $Mn_2Co_{0.5}Ni_{0.5}Ga$ have forms quite similar to that for Mn_2NiGa. This indicates that Co occupying the Ni sites hardly changes either the total DOS or that for the individual atoms Mn, Ni, and Ga, as shown in Fig. 7. As yet more Co is substituted for Ni, the ferrimagnetic structure is still retained, even when Co totally replaces the Ni in the Mn_2CoGa compound.[10] Turning to the case in which Co substitutes for Ga as in Model4, it has been found that the magnetic moments
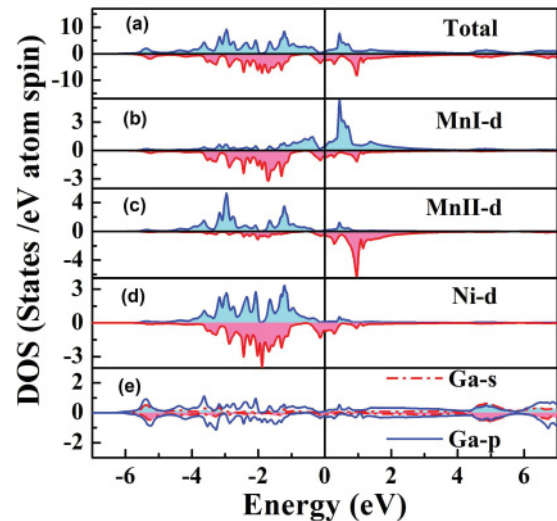

FIG. 6. (Color online) Calculated spin-projected DOS plots for the Mn_2NiGa alloy with atomic Model1. (a) The total DOS, (b) the partial DOS of the d component for MnI, (c) MnII, (d) Ni, and (e) Ga atoms are illustrated. The upper halves of each panel display the spin-up states.

of the MnD atoms are ferromagnetically aligned with those of the MnII atoms, as shown in Fig. 8, which clearly answers the question as to why the magnetization is so dramatically enhanced as to show the polymorphic magnetization behavior shown in Fig. 1.

More importantly, our calculation also indicates that, due to the Co dopant, the d-DOS of the Mn becomes broader in Model2 and Model4, especially in the latter case where the DOS distributions for the spin-up electrons of MnD and MnII are much broader than those in Model1 and Model2, as shown

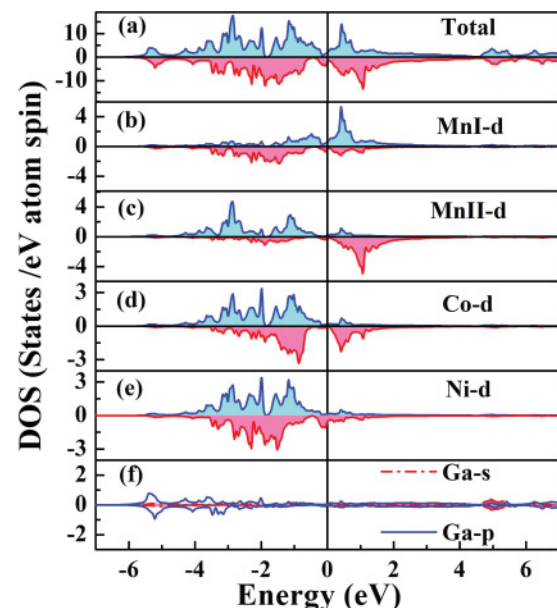

FIG. 7. (Color online) Calculated spin-projected DOS plots for the $Mn_2Co_{0.5}Ni_{0.5}Ga$ alloy with Model2. (a) The total DOS, (b) the partial DOS of the d component for MnI, (c) MnII, (d) doped Co, (e) Ni, and (f) Ga atoms are illustrated.
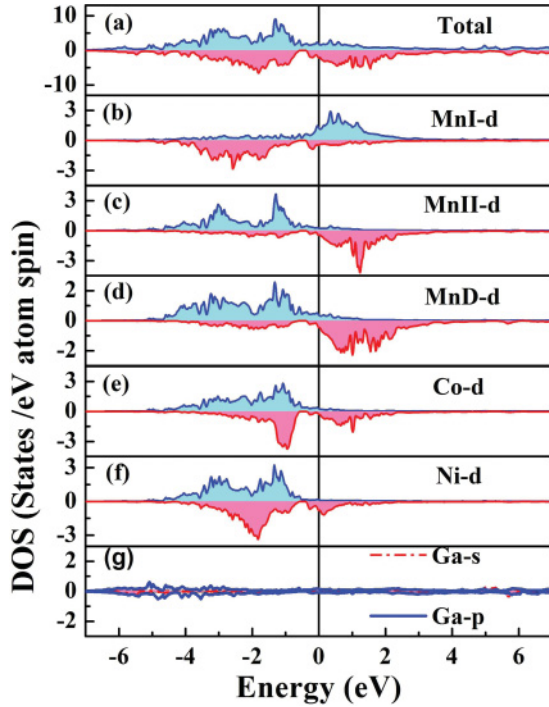
FIG. 8. (Color online) Calculated spin-projected DOS plots for the $Mn_2Co_{0.5}NiGa_{0.5}$ alloy with Model4. (a) The total DOS, (b) the partial DOS of the d component for MnI, (c) MnII, (d) MnD at D site, (e) Co at A site, (f) Ni, and (g) Ga atoms are illustrated.

in Figs. 6–8. This suggests that Mn d electrons have a higher level of hybridization with Co $3d$ electrons and are not so localized as in Mn_2NiGa and that there exists an enhanced exchange interaction[28] between the Mn and Co atoms in this atomic configuration. We believe that this is the physical mechanism for MnD switching from an antiferromagnetic to a ferromagnetic coupling with MnII, after undergoing an occupation change from the A site to the D site.

Table II collects the calculated and experimentally measured molecular moments, as well as the calculated moments of each atom for some typical MnCoNiGa alloys with the corresponding atomic configuration models shown in column two. The table allows five important conclusions to be drawn for the three atomic configurations: (1) For all compositions, the MnI and MnII atoms carry quite large but different magnetic moments of about -2.5 and 3.5 μ_B, respectively. This is because the MnII atoms have eight magnetic atoms (four MnI and four Ni atoms) as their nearest neighbors (denoted

as 1nn) as in a cubic crystal field, whereas the MnI atoms have only four magnetic atoms (four MnII atoms) neighbors as in a tetragonal crystal field.[29] (2) The Co and Ni atoms have positive moments of about 1.1–1.3 μ_B and 0.2–0.4 μ_B, respectively. Usually the sublattice formed by the MnI atoms is referred to as the antiferromagnetic sublattice and that formed by the MnII, Co, and Ni atoms as the ferromagnetic one. (3) These two sublattices compose a native ferrimagnetic structure in the alloy system which cannot be changed by Co substituting for Ni in Model2, and thus no apparent enhancement of magnetization and a small Δm_{Ni} are observed, as shown in Fig. 1. (4) When Co substitutes for Ga in the manner of Model4, some MnI atoms become MnD as mentioned before, and their moment value increases from about 2.6 to 3.6 μ_B (and). Meanwhile, their moment sign changes from negative to positive. These changes result in the MnI atom with a relatively small moment being removed from the antiferromagnetic lattice and then added into the ferromagnetic lattice as MnD with a relatively large moment. This simultaneously enlarges the ferromagnetic lattice and shrinks the antiferromagnetic lattice and dramatically enhances the magnetization, showing a quite large Δm_{Ga}. (5) Calculations using Model3 produce an anomalous negative moment for Co and an abnormally low total moment, far from the experimental value, indicating that the configuration of Model3 is not realized in these alloys.

These conclusions clearly indicate that the polymorphic magnetization behavior actually originates with the change of the magnetic structure due to the selective occupation of the Co atoms when the system is chemically doped.

D. Exchange interaction and local ferromagnetic structure

In this section, we discuss the coupling of the atomic moments using the theories proposed by Stearns and attempt to elucidate how a local ferromagnetic structure can be achieved.

Stearns *et al.* have systemically investigated the exchange interaction in Heusler alloys and have arrived at a number of important conclusions: (1) The transition metals Mn, Fe, Co, and Ni have a small portion of itinerant $3d$ (d_i) electrons per atom, and the larger the atomic number, the fewer d_i electrons they have;[30] (2) the higher the number of d_i electrons and the higher the conduction electron polarization (CEP), the stronger the exchange interaction;[31] (3) the Coulomb exchange between localized $3d$ (d_l) electrons and d_i electrons dominates the magnetism in Heusler alloys;[32] (4) the sign of the d_i electron polarization has an oscillatory behavior related to the interatomic distance.[31] Based on (4) above, a simplifying

TABLE II. The calculated and experimentally measured molecular moments, M_{Cal} and $M_{Exp.}$ and the calculated atomic moments for MnCoNiGa alloys with typical compositions (column one) and the corresponding atomic configuration models (column two).

Composition	Model	MnI	MnII	MnD	Ni	Co	Ga	$M_{Cal.}$	$M_{Exp.}$
$Mn_2Co_{0.25}Ni_{0.75}Ga$	2	-2.39	3.38		0.24	1.14	0.02	1.48	1.52
$Mn_2Co_{0.5}Ni_{0.5}Ga$	2	-2.34	3.34		0.24	1.08	0.02	1.68	1.70
$Mn_2Co_{0.25}NiGa_{0.75}$	3	-2.72	3.47		0.28	-1.66	0.04	0.65	
$Mn_2Co_{0.5}NiGa_{0.5}$	3	-2.72	3.41		0.34	-1.52	0.04	0.29	
$Mn_2Co_{0.25}NiGa_{0.75}$	4	-2.62	3.44	3.58	0.32	1.14	0.04	3.01	3.11
$Mn_2Co_{0.5}NiGa_{0.5}$	4	-2.58	3.53	3.63	0.40	1.28	0.04	5.12	5.29

assumption has been made, in this paper, that it is sufficient to consider just the 1nn and next nearest neighbor (denoted as 2nn) exchange interactions. As the d CEP falls off very rapidly with interatomic distance, this assumption is reasonable.[31] For investigating the exchange interaction in the Heusler alloy Mn_2NiGa, the Stearns theory is a suitable basis because it not only takes into account the atomic configuration, but also the variation with interatomic distance.

In MnCoNiGa compounds, based on conclusion number (2) above, when the interatomic distances between Mn, Co, and Ni atoms are equal, the atomic pair Mn-Mn has the highest exchange interaction, and the strength tends to decrease in the sequence Mn-Mn > Mn-Co > Mn-Ni. In addition, based on conclusion number (4) above, the exchange interaction is weaker between 2nn than between 1nn. Therefore, it is possible that the interatomic distance plays an important role in alternating the type of the exchange interaction, antiferromagnetic or ferromagnetic, between the atomic pairs Mn-Mn and Mn-Co in our MnCoNiGa system. This prediction has been confirmed by the recent report on the exchange interaction calculation for Mn2CoZ compounds.[33] Below, we will see that a local ferromagnetic structure can be achieved due only to a change in the interatomic distance.

From Fig. 4, one can see the interatomic distance relationships for the 1nn and 2nn in $Mn_2Ni_{0.5}Co_{0.5}Ga$ (Model2) and $Mn_2NiCo_{0.5}Ga_{0.5}$ (Model4) alloys. In the $Mn_2Ni_{0.5}Co_{0.5}Ga$ alloy, the MnI atoms are 1nn of the MnII atoms and 2nn of the Ni and doped Co atoms as shown in Fig. 4(b). The 1nn and 2nn interatomic distances are 2.5453 and 2.9391 Å, respectively. Therefore, in this case, the exchange interaction between MnI and MnII atoms is stronger than the others based on Stearns theories, which makes the MnI and MnII couple in an antiparallel manner. This is also the mechanism for the antiferromagnetic sublattice coupling in an antiparallel fashion with the ferromagnetic sublattice and exhibiting a native ferrimagnetic structure in our systems because these two sublattices are in a 1nn distance. Therefore, when Co substitutes for Ni, there is no change in the native ferrimagnetic structure of the system. In a similar way, all other Hg_2CuTi-type Mn_2YZ Heusler alloys whose atomic configuration follows Model1 are also the ferrimagnetic.

On the other hand, as shown in Fig. 4(d), when the Co substitutes for Ga in $Mn_2NiCo_{0.5}Ga_{0.5}$ compounds, the system takes up the atomic configuration of Model4. One may notice that the only structural difference from Model2 is that two Co atoms occupy the MnI sites, and the corresponding MnI atoms

move to the vacant Ga (D) sites, becoming MnD atoms. In this case, a new atomic configuration is generated around the doped Co atom in which the MnII and MnD atoms become 2nn to each other at a distance of 2.9391 Å, and both of them are 1nn of the doped Co at a relatively small distance of 2.5453 Å. This conversion of the distance relationship makes the exchange interactions between Co-MnII/MnD stronger than that of MnII-MnD. This corresponds to the apparently widened d-DOS distribution (a higher hybridization between Co and Mn 3d electrons), as shown in Fig. 8. Thus, an additional ferromagnetic coupling between Co and MnD is achieved, which in turn generates a local ferromagnetic structure of MnII-Co-MnD in the system. This is similar to the magnetic structure in $Co_2Mn_{1+x}Ga_{1-x}$ observed through hyperfine field measurements.[34] It should be pointed out that the local ferromagnetic structure is generated only locally in the small volume in which the atomic relationship must be 2nn for MnD-MnII and must be 1nn for Co-MnD and Co-MnII. This critical condition indicates the importance of the atomic distance, as we have indicated in our previous work.[8]

E. Behavior of the local ferromagnetic structure across the crystallographic and magnetic transition

As we have discussed above, the local ferromagnetic structure in a bcc structure (the parent phase of ferromagnetic shape memory alloys) enables the system to have a high magnetization, which realizes one of two conditions for having a large ΔM in FSMAs. The other condition, as we have observed in many ferromagnetic shape memory alloys,[1–7] is that the magnetization should significantly decrease when the alloys transform to the martensitic phase. This implies that the local ferromagnetic structure should not survive through this crystallographic transition. The MnNiCoGa martensitic phase with a tetragonal structure is derived from its bcc parent phase via changes in the lattice parameters. Through the transformation, the corresponding change of interatomic distance is shown in Table III. One can see that the 1nn MnD (MnII)-Co distance slightly increases to the extent of 0.64% from 2.5579 to 2.5745 Å, while the interatomic distance between the 2nn MnII-MnD dramatically decreases by 6.4% from 2.9536 to 2.7636 Å. The relative change in the distance for the latter case is, therefore, 10 times larger than the former. Considering that there is a critical distance of about 2.8 Å for an antiferromagnetic coupling between Mn atoms in α-Mn and β-Mn,[35] it is reasonable to suppose that the disappearance

TABLE III. The change in the interatomic distances through the martensitic transformation when the system takes the form of Model4 for the MnCoNiGa system. The lattice parameters are taken from our previous report on Mn_2NiGa.[9]

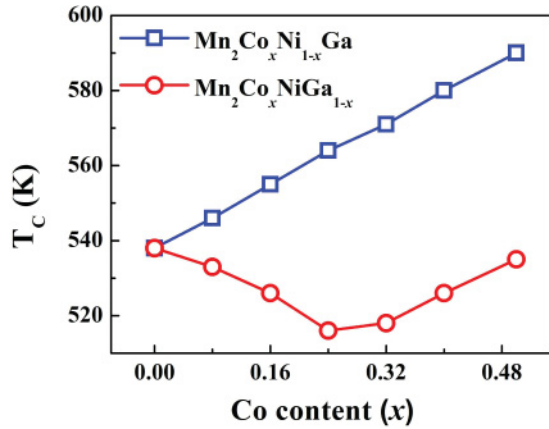| Corresponding atom pairs	Lattices (Å)	First neighbor		Second neighbor
		MnI-MnII	MnII/MnD-Co	MnII-MnD
Parent	5.9072		2.5579	2.9536
Martensite	5.5272(a)		2.5745	2.7636
	5.5272(b)			
	6.7044(c)			
Bond-length change (Å)			0.017	−0.190
Change ratio (%)			0.64	6.4

FIG. 9. (Color online) The dependence of the Curie temperature (T_c) on the Co content in the $Mn_2Co_xNi_{1-x}Ga$ and $Mn_2Co_xNiGa_{1-x}$ systems.

of the local ferromagnetic MnII-Co-MnD structure in the martensite is mainly due to the significant decrease in the MnII-MnD distance, rather than the negligible increase in the MnD(MnII)-Co distance. With this decrease in the interatomic distance, the moments of MnD and MnII revert to the antiparallel arrangement, and the local ferromagnetic structure converts to the ferrimagnetic structure. Without a change in the Co content, this is also a polymorphic magnetization behavior caused by the variation of atomic distance, which also plays an important role for the exchange interaction effect in the martensitic system.

Figure 9 shows the composition dependence of the Curie temperature, T_C, in the two series of substitution samples we have studied. When Co substitutes for Ni, the T_C monotonically increases with increasing Co. This should be attributed to the fact that the Mn-Co exchange interaction is stronger than that of Mn-Ni in this ferrimagnetic system. This suggests that, in Mn2YZ-based Heusler alloys, both of the antiferromagnetic and ferromagnetic lattices mutually determine the T_C. Therefore, when the local ferromagnetic structure appears by substituting Co for Ga, an interesting composition dependence of T_C can be observed, as shown in Fig. 9: it initially decreases on the low Co content side and then starts to increase at about $x = 0.24$. Based on the above discussion, the decrease in T_C should be attributed to the partial destruction of the antiferromagnetic lattice due to the appearance of the local ferromagnetic structure. On the other hand, the subsequent increase in T_C indicates another dominating effect: the ferromagnetic lattice is enhanced by

increasing the local ferromagnetic structure. The switch in the dominating role for the two lattices occurs at about $x = 0.24$ and results in a minimum of T_C, where each crystallographic unit cell contains one Co atom on average. This is also the composition at which the moment increment of Δm_{Ga}, increases from 6.79 to 8.85 μ_B (when $x = 1$) in $Mn_2Co_xNiGa_{1-x}$ alloys, which implies a stronger exchange interaction caused by more Co atoms entering into the unit cell at the A sites.

IV. CONCLUSION

A polymorphic magnetization behavior, in which the magnetization can be changed by a factor of three, has been observed in MnCoNiGa alloys in which Co has been substituted for the Ni or Ga. The effects of the exchange interaction have been investigated based on the corresponding atom configuration generated by the occupation selectivity of the doped Co atoms. Our calculations show that a high level of d-electron hybridization can occur when the Mn atoms are nearest neighbors to a Co atom. This causes a strong ferromagnetic exchange interaction between them in specific atomic configurations and produces a local ferromagnetic structure in the native ferrimagnetic matrix. The local ferromagnetic structure simultaneously enlarges the ferromagnetic lattice and shrinks the antiferromagnetic one, thereby increasing the magnetization and resulting in the observed polymorphic magnetization behavior. Consequently, based on the theoretical work of Stearns, the necessary condition for achieving the local ferromagnetic structure has been confirmed: surrounding the doped Co atoms, the atomic relationship should be 1nn for Co-Mn and 2nn for Mn-Mn. Based on the critical role of the interatomic distances, the disappearance of the local ferromagnetic structure in a tetragonal martensitic structure has been attributed to the significant shrinkage of the distance between 2nn Mn-Mn atoms, which results in the local ferromagnetic structure recovering antiferromagnetic coupling. Due to its existence in the native ferrimagnetic structure, the local ferromagnetic structure results in an abnormal composition dependence for T_C.

*ghwu@iphy.ac.cn

[1] R. Kainuma, Y. Imano, W. Ito, Y. Sutou, H. Morito, S. Okamoto, O. Kitakami, K. Oikawa, A. Fujita, T. Kanomata, and K. Ishida, Nature **439**, 957 (2006).

[2] K. Koyama, H. Okada, K. Watanabe, T. Kanomata, R. Kainuma, W. Ito, K. Oikawa, and K. Ishida, Appl. Phys. Lett. **89**, 182510 (2006).

[3] R. Kainuma, Y. Imano, W. Ito, H. Morito, Y. Sutou, K. Oikawa, A. Fujita, K. Ishida, S. Okamoto, O. Kitakami, and T. Kanomata, Appl. Phys. Lett. **88**, 192513 (2006).

[4] S. Y. Yu, L. Ma, G. D. Liu, Z. H. Liu, J. L. Chen, Z. X. Cao, G. H. Wu, B. Zhang, and X. X. Zhang, Appl. Phys. Lett. **90**, 242501 (2007).

[5] S. Y. Yu, Z. X. Cao, L. Ma, G. D. Liu, J. L. Chen, G. H. Wu, B. Zhang, and X. X. Zhang, Appl. Phys. Lett. **91**, 102507 (2007).

[6] L. Ma, H. W. Zhang, S. Y. Yu, Z. Y. Zhu, J. L. Chen, G. H. Wu, H. Y. Liu, J. P. Qu, and Y. X. Li, Appl. Phys. Lett. **92**, 032509 (2008).

[7] R. Kainuma, W. Ito, R. Y. Umetsu, K. Oikawa, and K. Ishida, Appl. Phys. Lett. **93**, 091906 (2008).

⁸L. Feng, L. Ma, Z. Y. Zhu, W. Zhu, E. K. Liu, J. L. Chen, G. H. Wu, F. B. Meng, H. Y. Liu, H. Z. Luo, and Y. X. Li, J. Appl. Phys. **107**, 013913 (2010).

⁹G. D. Liu, J. L. Chen, Z. H. Liu, X. F. Dai, G. H. Wu, B. Zhang, and X. X. Zhang, Appl. Phys. Lett. **87**, 262504 (2005).

¹⁰G. D. Liu, X. F. Dai, H. Y. Liu, J. L. Chen, Y. X. Li, G. Xiao, and G. H. Wu, Phys. Rev. B **77**, 014424 (2008).

¹¹O. K. Andersen, Phys. Rev. B **12**, 3060 (1975).

¹²M. Weinert, E. Wimmer, and A. J. Freeman, Phys. Rev. B **26**, 4571 (1982).

¹³P. E. Blochl, O. Jepsen, and O. K. Andersen, Phys. Rev. B **49**, 16223 (1994).

¹⁴S. R. Barman, S. Banik, A. K. Shukla, C. Kamal, and A. Chakrabarti, Epl **80**, 57002 (2007).

¹⁵G. D. Liu, X. F. Dai, S. Y. Yu, Z. Y. Zhu, J. L. Chen, G. H. Wu, H. Zhu, and J. Q. Xiao, Phys. Rev. B **74**, 054435 (2006).

¹⁶Y. Sutou, Y. Imano, N. Koeda, T. Omori, R. Kainuma, K. Ishida, and K. Oikawa, Appl. Phys. Lett. **85**, 4358 (2004).

¹⁷H. C. Kandpal, G. H. Fecher, and C. Felser, J. Phys. D **40**, 1507 (2007).

¹⁸M. Pugaczowa-Michalska, A. Go, L. Dobrzynski, and S. Lipinski, J. Magn. Magn. Mater. **256**, 46 (2003).

¹⁹P. J. Webster, Contemp. Phys. **10**, 559 (1969).

²⁰Y. Feng, J. Y. Rhee, T. A. Wiener, D. W. Lynch, B. E. Hubbard, A. J. Sievers, D. L. Schlagel, T. A. Lograsso, and L. L. Miller, Phys. Rev. B **63**, 165109 (2001).

²¹T. J. Burch, T. Litrenta, and J. I. Budnick, Phys. Rev. Lett. **33**, 421 (1974).

²²R. B. Helmholdt and K. H. J. Buschow, J. Less-Common Met. **128**, 167 (1987).

²³H. Z. Luo, H. W. Zhang, Z. Y. Zhu, L. Ma, S. F. Xu, G. H. Wu, X. X. Zhu, C. B. Jiang, and H. B. Xu, J. Appl. Phys. **103**, 083908 (2008).

²⁴K. Ozdogan, I. Galanakis, E. Sasioglu, and B. Atkas, J. Phys. Condens. Matter **18**, 2905 (2006).

²⁵R. Weht and W. E. Pickett, Phys. Rev. B **60**, 13006 (1999).

²⁶C. Jiang, M. Venkatesan, and J. M. D. Coey, Solid State Commun. **118**, 513 (2001).

²⁷H. Z. Luo, Z. Y. Zhu, L. Ma, S. F. Xu, X. X. Zhu, C. B. Jiang, H. B. Xu, and G. H. Wu, J. Phys. D **41**, 055010 (2008).

²⁸S. Picozzi, A. Continenza, and A. J. Freeman, Phys. Rev. B **66**, 094421 (2002).

²⁹R. C. O'Handley, *Modern Magnetic Materials: Principles and Applications* (Wiley, New York, 1999), pp. 174.

³⁰M. B. Stearns, Phys. Rev. B **8**, 4383 (1973).

³¹M. B. Stearns and J. M. Norbeck, Phys. Rev. B **20**, 3739 (1979).

³²J. R. Reitz and M. B. Stearns, J. Appl. Phys. **50**, 2066 (1979).

³³M. Meinert, J. Schmalhorst, and G. Reiss, J. Phys. Condens. Matter **23**, 116005 (2011).

³⁴L. D. Khoi, P. Veillet, and I. A. Campbell, J. Phys. F **8**, 1811 (1978).

³⁵J. S. Kasper and B. W. Roberts, Phys. Rev. **101**, 537 (1956).